Similarity learning hidden semi-Markov model for adaptive prognostics of composite structures

Eleftheroglou, Nick; Galanopoulos, Georgios; Loutas, Theodoros

DOI
10.1016/j.ress.2023.109808

Publication date
2024

Document Version
Final published version

Published in
Reliability Engineering and System Safety

Reliability Engineering and System Safety 243 (2024) 109808

Contents lists available at ScienceDirect

Reliability Engineering and System Safety

journal homepage: www.elsevier.com/locate/ress

Similarity learning hidden semi-Markov model for adaptive prognostics of composite structures

Nick Eleftheroglou [a,b,*], Georgios Galanopoulos [b], Theodoros Loutas [b]

[a] Intelligent Sustainable Prognostics Group, Aerospace Structures and Materials Department, Faculty of Aerospace Engineering, Delft University of Technology, Kluyverweg 1, 2629HS Delft, the Netherlands
[b] Applied Mechanics Laboratory, Department of Mechanical Engineering and Aeronautics, University of Patras, 26504 Rio, Greece

ARTICLE INFO

Keywords:
Prognostics
Adaptive prognostics
Remaining useful life
Composites
Markov models
HSMM
PHM

ABSTRACT

Data-driven methodologies have found increasing usage in the last decade for remaining useful life (RUL) prognostics of composite materials utilizing structural health monitoring (SHM) data. Of particular interest is the reliable RUL prediction in cases where the end-of-life is not in between the extreme values within the testing dataset. For example, when unexpected phenomena that severely compromise the structural integrity occur during the service life. Such cases are often referred as outliers and the RUL prognosis based on a data-driven model that learns from past data is often erroneous. This study addresses this challenge by proposing a new stochastic model; the Similarity Learning Hidden Semi Markov Model (SLHSMM), an extension of the Non-Homogenous Hidden Semi Markov Model (NHHSMM). Through the utilization of a nonparametric discrete distribution, which characterizes the similarity between the testing structure and the training structures, a dynamic re-estimation process is employed. This process assigns higher importance to the training structures that display greater similarity to the testing one. As a result, the estimated parameters effectively capture the specific characteristics of the testing structure. The training and testing SHM data sets consist of strain measurements collected from a case study where carbon–epoxy single-stringered panels, are subjected to constant, variable, and random amplitude fatigue loading until failure. RUL estimations from the SLHSMM, the NHHSMM, and the Gaussian Process Regression (GPR) are compared. The SLHSMM clearly outperforms its classical counterpart and GPR providing more accurate outlier and inlier prognostics, demonstrating its capability to adapt to unexpected phenomena and integrate unforeseen data into a prognostic platform.

1. Introduction

Modern composite structures usually operate in demanding environments and variable operational conditions, e.g. operational loads, temperature, humidity which affect the way they degrade in an unknown manner. Inherent manufacturing flaws and defects tend to significantly affect their useful life and relevant studies have reported a huge scatter of the failure cycles after fatigue campaigns in coupons [1, 2] or hierarchically more complex structures like single-stringered coupons [3] of the same batch. In addition, the service life of a composite material is heavily influenced by the way it is operated, maintained, as well as the environmental and operation conditions, which are not always the designed ones, since unexpected phenomena can occur during the structure's lifetime. For the latter, let's consider an example from the aviation industry. Foreign object impacts, such as bird strikes, hail, tool drops, etc., may occur anytime during the lifetime of the aircraft. These events fall into the category of unexpected phenomena that may create damage, which has not been anticipated in the design phase. The implication of such an unexpected phenomenon to the integrity of the structural component could be severe and common practice, as long as the operators record the event, is to interrupt the aircraft operation and initiate inspection and repair actions resulting in unscheduled maintenance actions which incur extra costs, delays and reduced aircraft availability. Towards a condition-based maintenance paradigm shift in civil aviation, prognosis of the Remaining Useful Life (RUL) of structures as well as systems claim a central role. The concept relies on properly sensorized critical systems and structures for health monitoring purposes and the use of model-based or data-driven

* Corresponding author at: Intelligent Sustainable Prognostics Group, Aerospace Structures and Materials Department, Faculty of Aerospace Engineering, Delft University of Technology, the Netherlands.
E-mail address: n.eleftheroglou@tudelft.nl (N. Eleftheroglou).

https://doi.org/10.1016/j.ress.2023.109808
Received 7 February 2023; Received in revised form 7 November 2023; Accepted 8 November 2023
Available online 11 November 2023

methodologies to assess the damage and estimate the RUL.

RUL prediction models have been categorized as model-based, data-driven, and hybrid [4]. Despite a few phenomenological approaches that have been proposed to model composite materials degradation during their service life we are still far from a complete physical model of this complex process which asks for probabilistic approaches rather than deterministic ones. Therefore, the efforts during the last years have been directed to data-driven approaches for RUL prognosis in composite materials utilizing probabilistic or machine learning models as shown in [1,2,5,6].

Data-driven models though have limitations related to their ability to predict RUL efficiently and they are usually successful when the testing data are rather close and relevant to the training data. For example, in the case where we want to estimate the RUL of a composite structure experiencing foreign object impact, we have to include in the training of our model(s) data coming from a similar impact scenario. In other words, a data-driven model performs well when the testing dataset resembles the training dataset. Creating a training database covering all the possible real-life scenarios is impractical though. There is a strong need to develop prognostic models with real-time adaptivity capabilities in order to predict more accurately the RUL of composite structures that experience unexpected phenomena during their service life. Nevertheless, there is quite limited literature available about adaptive prognostics in general.

Most of the recent studies in prognostics have focused on treating the prognostic task as a regression problem, utilizing advanced machine learning algorithms like Long-Short-Term-Memory (LSTM) networks [7], Bayesian Deep Learning [8], Convolutional Neural Networks (CNN) [9], Recurrent Neural Networks (RNN) [10], and Temporal Flow Transformers [11]. These machine learning algorithms have successfully dealt with prognostic tasks, even with the lack of interpretability as they are mostly black-box models. However, an alternative approach to estimate the remaining useful life (RUL) is through stochastic modeling of the degradation history of the engineering asset.

In this direction, Zhang et al. [12] proposed a systematic method for degradation modeling and RUL prediction based on an uncertain process for degradation with a recovery phenomenon. Initially, an uncertain process is adopted to model degradation and account for epistemic uncertainty. Subsequently, a novel method based on similarity and uncertain weighted least squares estimation is proposed to update the model parameters using real-time monitoring data. Zhang [13] proposed a novel model for RUL prediction of deteriorating products operating under dynamic environments. The environmental effects are classified into two aspects: the impacts from the measurable covariate and the impacts from the unobservable factors. The model incorporates the impacts of both kinds of factors into the Wiener process degradation model, where the measurable covariate is modeled by an Ornstein–Uhlenbeck process, and the effect of the unobservable factors is modeled by a stochastic degradation rate using a Brownian motion. The model parameters are estimated using the Maximum Likelihood Estimation (MLE) method. The hidden degradation rate is inferred using the Kalman filter, and a simulation-based algorithm is proposed for RUL prediction.

Pang et al. [14] used a nonlinear diffusion process model in an age- and state-dependent framework to characterize the degradation process, accounting for unit-to-unit variability. A state space model is constructed to associate the hidden degradation states with the measurement errors. The degradation states and the unknown parameters are estimated using the Extended Kalman Filter and the Expectation-Maximization algorithm.

Yu et al. [15] proposed a generalized Wiener process-based degradation model with an adaptive drift to capture nonlinearity, temporal uncertainty, item-to-item variability, and time-varying degradation. A recursive Bayesian filtering algorithm is derived to update the drift distribution. The expectation-maximization algorithm is utilized to estimate all other model parameters online whenever new degradation measurements from the system under consideration are available, without requiring population-based degradation data from identical systems in the same batch.

Liao et al. [16] proposed a multi-phase degradation model based on the Wiener process to characterize the multi-phase characteristics of the degradation signals. All model parameters are assumed to be random variables to account for unit heterogeneity, including the change-point locations, corresponding abrupt jumps at the change points, drift parameters, and diffusion parameters of each phase. Then, the Bayesian approach is utilized to integrate available data with historical data. Furthermore, considering the uncertainties of the change points and abrupt jumps, the probability density function of RUL is obtained for predicting RUL.

Orchard et al. [17] utilized two different approaches for outer feedback correction loops in particle filters algorithms. These loops incorporate information for the short-term prediction error to improve the performance of the overall prognostic framework. However, important initialization parameters such as the number of prediction steps (k), and the variance vector of the kernel noise $[p\ q]^T$ have to be predefined. Both approaches were tested using data from an artificial fault test in a critical component of a rotorcraft transmission system. Results show that outer feedback correction loops improve the precision and accuracy of the predicted RUL.

Sbarufatti et al. [18] proposed a model for battery prognostics, which is a combination of particle filters and radial basis function neural networks (RBFNNs). This model could be considered adaptive as the RBFNNs are trained online. More specifically the neural network parameters are identified online by the particle filters as soon as new observations of the battery terminal voltage become available. The RBFNNs algorithm has been able to provide satisfactory prognostic predictions over normal and aging scenarios. Prior to the utilization of RBFNNs, artificial noise was introduced to the dataset to replicate realistic online voltage measurements, simulating real-world conditions rather than controlled environment settings. Determining the appropriate noise variances is a challenging task, as excessively small values may impede effective state-space exploration, while excessively large values may hinder efficient state estimation.

Furthermore, in Khan et al. [19] an adaptive degradation prognostic model, utilizing particle filters with a neural network degradation model, was proposed in order to predict the RUL of turbofan jet engines. The RUL predictions were generated using two different algorithms for benchmarking the results, the nominal RBFNNs with particle filters and the similarity-based prognostics. The RUL predictions for both algorithms are characterized by volatility but more importantly, the similarity-based approach does not support the prediction of RUL confidence intervals which is an essential output for the robustness of the algorithm. Furthermore, the proposed prognostic model requires the initialization of the random walk step size (σa). The σa selection is not a straightforward choice, since a large value will result in fast convergence but high fluctuations whereas a small value will produce a smoother but slower convergence of the parameter estimation process, and at the same time is an important selection regarding the final prognostics. As a result, the selection of σa is driven by the case study.

Daroogheh et al. [20] proposed a hybrid prognosis model, which integrates particle filters and neural networks for gas turbine engines. It is worth mentioning that the integration of particle filters and neural networks is a common combination in the literature since both of these algorithms are available in many commercial and open-source programming languages and their implementation is relatively easy with respect to other algorithms. The authors developed a hybrid prediction model based on extending particle filters to the future time horizon by utilizing an observation forecasting scheme. This scheme utilizes a neural network approach as a nonlinear time series forecasting method. Neural networks are trained adaptively based on the newly received data in the case that the deviations between the forecasted observation from this network and the real observation increase from one test data to another test data set. Nonetheless, the main disadvantage of this hybrid prognosis model is the absence of confidence intervals.

Si et al. [21] utilized a Wiener-process-based model with a recursive filter algorithm for RUL predictions. A state space model updates the drift coefficients, which are defined as random variables, and an expectation maximization (EM) algorithm re-estimates all the unknown parameters as soon as new data is available. The proposed model is applied to estimate the RUL of gyros in an inertial navigation system. The proposed model of Si et al. excels in most of the cases that are presented in [22] and [23]. However, Wiener models assume that the degradation process of the studied system and the operation time are linearly connected, which is not always the case.

In the field of structural adaptive prognostics the existing literature is very limited. Cadini et al. [24] proposed to exploit the flexibility of neural networks so as to adaptively learn from a monitored metallic structure and derive models for diagnostics and prognostics in real-time. In order to achieve that, neural networks are embedded within a particle filtering scheme and the training process of the network is performed in real-time as SHM data become available during the structure's operation. As a result, the proposed RUL model is capable of sequentially updating itself utilizing the available CM data. This model was demonstrated on simulated and real fatigue crack growth tests of metallic aeronautical panels. The main limitations of this model are the required convergence time to the actual RUL, which tends to be larger than similar RUL models, the volatile RUL predictions, and the divergent behavior of confidence intervals towards the end of life. However, the proposed model could play a role in structural prognostics in the future when physics-based or more accurate empirical/phenomenological models become available.

Finally, Eleftheroglou et al. [6] proposed the Adaptive Non-Homogenous Hidden Semi Markov Model (ANHHSMM), an extension of the classical Non-Homogenous Hidden Semi Markov Model (NHHSMM). The ANHHSMM uses diagnostic measures, which are estimated based on the training and testing SHM data, and it adapts the trained degradation process parameters vector. The training data set was collected from open-hole carbon–epoxy specimens, subjected to fatigue loading, while the testing data set was collected from specimens, subjected to fatigue and *in-situ* impact loading. The ANHHSMM provided improved predictions in comparison to the NHHSMM, demonstrating its capability to adapt to unexpected phenomena and integrate unforeseen data into the prognostics course. However, the suggested model is able to adapt only part of its parameters i.e. the degradation process parameters when the observation process parameters are predefined.

Based on the aforementioned literature review, the need to develop new mathematical models with real-time adaptivity capabilities emerges, which will be able to predict more accurately the RUL of composite structures in cases where unexpected phenomena may occur during the service life. To that end, the present study makes a significant contribution by introducing a novel adaptive prognostic model known as the Similarity Learning Hidden Semi Markov Model (SLHSMM). It is worth mentioning that the decision to develop a new version of the NHHSMM was driven by the model's demonstrated superior prognostic capabilities compared to other prognostic models. Loutas et al. compared the NHHSMM with gradient-boosted trees (GBTs) and Bayesian feed-forward neural networks (BNNs). The first study [25] predicted the RUL of reciprocating compressors using temperature as a health indicator, while the second study [5] predicted the RUL of composite structures under fatigue loading using acoustic emission measurements as health indicators. In both benchmark studies, the NHHSMM outperformed GBTs and BNNs in terms of multiple metrics and provided more consistent predictions. As a result, the development of an adaptive extension of the NHHSMM, which is a generic version of Markov models (MMs), has shown significant promise. This adaptive extension allows for the adaptation of all training parameters, rather than just a subset of them as seen in the ANHHSMM approach.

MMs have been utilized since the 1960s [26], but the main assumption of this model is that the degradation process of an engineering system can be directly observed. However, in reality, this is not often the case for most engineering systems, as the degradation process is typically a hidden or latent process that can only be inferred indirectly through condition monitoring data. Driven by that drawback, Hidden Semi Markov models (HMMs) have been introduced by Rabiner [27]. HMM is a multistate structure where each state is hidden and can be correlated to the observed condition monitoring data. HMMs provide an advantage of interpretability compared to "black-box" methods like artificial neural networks commonly used in advanced prognostic models. However, HMMs assume exponentially distributed state durations (sojourn time), which is not always realistic. Hidden Semi Markov models (HSMMs) relax this assumption [28], allowing for flexible modeling of sojourn times. Both in HMMs and HSMMs, there is a limitation regarding the state transition which is independent on the age of the engineering system or the sojourn time in the current hidden state. To take into account this limitation Moghaddass, and Zuo [29] extended the HSMM approach developing the Non-Homogenous Hidden Semi Markov model (NHHSMM). According to NHHSMM, state transitions become dynamic and depend on the current hidden state, sojourn time, total age of the asset, or any combination of these parameters. Peng and Dong [30] also extended HSMMs to NHHSMMs using an iteration algorithm, introducing aging factors in the transition matrix obtained from HSMM. They presented three types of aging factors: constant, multiple, and exponential forms. The work of Moghaddass and Zuo [29], on the other hand, doesn't impose any limitations on the dependency between state transitions and aging parameters. Hence, it can be considered the most generic approach in the literature on Markov models. NHHSMM stands out in several aspects, including being a data-driven approach without sojourn time limitations compared to other available prognostic models.

The remainder of this paper is organized as follows: the SLHSMM is described in Section 2, the case study analysis is presented in Section 3 and finally, the paper is concluded in Section 4.

2. Methodology

Methods based on stochastic filtering [31], multi-stage degradation models [32], and covariate hazard models [33] are common methodologies, which can take lifetime scattering into account [21]. Since the phenomenon of damage accumulation of composite structures is stochastically correlated with SHM data, multi-stage degradation models, such as the NHHSMM, are the preferable approach to estimate the RUL of composite structures.

The NHHSMM model [29] consists of two processes the degradation process with parameters $\mathbf{\Gamma}$ and the observation process with parameters $\mathbf{B}$. $\mathbf{\Gamma}$ parameters characterize the distribution of sojourn times. They specifically represent the probability density functions that describe the duration for which the system remains in a particular hidden state before transitioning to the next one. Additionally, the degradation process $\mathbf{B}$ parameters establish the relationship between the observed data, in our case, SHM data, and the hidden states. Collectively, these parameters, expressed as the set $\boldsymbol{\theta}=\{\mathbf{B}, \mathbf{\Gamma}\}$, comprehensively define the NHHSMM model. According to this model, the degradation process depends on the current hidden state, the sojourn time of the current hidden state, and the total age of the studied system. However, a limitation of this model is the lack of adaptation regarding the estimated model's parameters $\boldsymbol{\theta}=\{\mathbf{B}, \mathbf{\Gamma}\}$, while the engineering system under monitoring e.g. a composite structure, is operating. To tackle the adaptation issue, the ANHHSMM was proposed by Eleftheroglou et al. [6]. However, the ANHHSMM model can adapt only the degradation process parameters $\mathbf{\Gamma}$ without allowing any adaptation capability to the observation process parameters $\mathbf{B}$. In this respect, we develop and propose a new adaptive version of the NHHSMM, i.e. the Similarity Learning HSMM (SLHSMM), which will be capable of adapting not only the degradation process parameters ($\mathbf{\Gamma}$) but also the observation process parameters (**B**).

The flowchart presented in Fig. 1 illustrates the steps involved in the proposed model. To initiate the process, both the SHM training data and real-time testing data are required. The first step involves calculating the similarity between the testing system and the training ones. This similarity measure plays a crucial role in the subsequent steps. By incorporating this similarity information into the likelihood function, the estimated parameters **Γ*** and **B*** can be optimized to better describe the characteristics of the testing system. Notably, more weight is assigned to the training systems that exhibit higher similarity to the testing system, enhancing the model's ability to capture its specific characteristics. Once the parameters **Γ** and **B** have been estimated, the diagnostic and prognostic measures can be calculated based on these parameter values. These measures provide valuable insights into the current state and RUL of the testing system. Overall, the following flowchart demonstrates how the proposed model utilizes the available data, similarity calculations, and estimated parameters to perform diagnostic and prognostic assessments effectively.

2.1. Similarity learning HSMM

The SLHSMM consists of a bi-dimensional stochastic process. The first process forms a finite Semi-Markov chain, which is not directly observed, and the second process, conditioned on the first one, forms a sequence of independent observations, e.g. SHM data. In order to describe the aforementioned bi-dimensional stochastic process the model's parameters **θ={Γ,B}** have to be estimated via the available SHM data. **Γ** parameters characterize the transition rate distribution between the hidden states (degradation process), while **B** parameters deal with the correlation between the hidden states and SHM data (observation process). This correlation is represented in a nonparametric and discrete form via a matrix called emission matrix.

$$\omega^{r}_{1,1}(\boldsymbol{\theta}_{\mathbf{old}},\boldsymbol{\theta}) = \sum_{k=1}^{K} w_T^{(k)} \text{ x } \left(\Pr\left(y^{(k)}\middle|\boldsymbol{\theta}_{\mathbf{old}},\zeta\right)\right)^{-1} \times \sum_{j=1}^{N}\sum_{a=0}^{d_k}\sum_{d=1}^{d_k-a} \log(\varepsilon_a^{(k)}(r,j,d|\boldsymbol{\theta},\zeta) \times \kappa_a^{(k)}(r,j,d,y^{(k)}|\boldsymbol{\theta}_{\mathbf{old}},\zeta) \tag{3}$$

The parameter estimation process consists of the initialization and training procedure. The purpose of the initialization procedure is to identify, with high computational efficiency, a set of parameters ζ which will associate the damage accumulation phenomenon and the available SHM data. The initialization procedure is obtained by defining the number of possible discrete degradation states (N), the transition diagram which defines the connectivity between the states and the allowed transitions (Ω), the transition rate's statistical function (λ), the SHM data of K training observation sequences y(k), and the discrete SHM indicator space (**Z**={z1,z2,…,zV}). This indicator space, denoted as **Z**, represents the potential set of V discrete values that the SHM data can assume. Subsequently, the continuous SHM degradation values are discretized by assigning each continuous value to its corresponding cluster. This transformation yields discrete degradation histories, a crucial step for computational efficiency.The reader can refer to Eleftheroglou and Loutas [1] for a more detailed description.

With regards to the training procedure, the model parameters **θ={Γ, B}** are obtained via a new similarity learning maximum likelihood estimation (SL-MLE) method. The similarity relationship between the testing and training degradation histories is dynamic and represented by a nonparametric discrete distribution, we shall refer to it as the similarity learning vector (SLV). The SLV is time-dependent and may have K elements, where the kth element of this vector quantifies the similarity of the testing degradation history and kth training degradation history up to time T ($w_T^{(k)}$). For similarity quantification, different methods can be used e.g. cosine similarity, Euclidean distance, Manhattan distance, etc. In this study, the Euclidean distance method is utilized due to its simplicity. A Euclidean SLV has elements that are obtained via Eq. (1).

$$w_T^{(k)} = \frac{\sum_{i=1}^{T}\left| z_i - y_i^{(k)}\right|}{\sum_{k=1}^{K}\sum_{i=1}^{T}\left| z_i - y_i^{(k)}\right|} \tag{1}$$

Where $\sum_{k=1}^{K} w_T^{(k)} = 1$, K is the available training degradation histories, z_i is the ith observation of the testing data, $y_i^{(k)}$ the ith observation of the kth degradation history of the training dataset and T is the similarity learning timestep.

The proposed SL-MLE leads to the maximization of the likelihood function $L(\boldsymbol{\theta},\mathbf{y}^{(1:K)})$, where $\mathbf{y}^{(k)}$ is the kth degradation history, K is the number of available degradation histories, **θ={Γ,B}** and $w_T^{(k)}$ is the kth SLV element at a predefined time step T.

$$L\left(\boldsymbol{\theta},\mathbf{y}^{(1:\mathbf{K})},T\right) = \prod_{k=1}^{K} w_T^{(k)} \text{ x } \Pr\left(y^{(\mathbf{k})}\middle|\boldsymbol{\theta},\zeta\right) \Rightarrow^{L'=\log(L)}$$

$$L'\left(\boldsymbol{\theta},\mathbf{y}^{(1:\mathbf{K})},T\right) = \sum_{k=1}^{K}\log\left(w_T^{(k)} \text{ x } \Pr\left(y^{(\mathbf{k})}\middle|\boldsymbol{\theta},\zeta\right)\right)\Rightarrow$$

$$\boldsymbol{\theta}^* = \arg\max_{\boldsymbol{\theta}}\left(\sum_{k=1}^{K}\log\left(w_T^{(k)} \text{ x } \Pr\left(y^{(\mathbf{k})}\middle|\boldsymbol{\theta},\zeta\right)\right)\right) \tag{2}$$

Utilizing Baum's auxiliary function [27] the above optimization task Eq. (2)) is reduced to a set of independent equations for the re-estimation of the parameters of **Γ** and **B**. Via Eqs. (3) and ((4) the degradation parameters **Γ** and observation parameters **B** can be estimated accordingly.

where $1 \le r \le N-1$.

$$b_i(q) = \frac{\sum_{k=1}^{K}\left(w_T^{(k)} \text{ x } \Pr\left(y^{(k)}\middle|\boldsymbol{\theta}_{\mathbf{old}},\zeta\right)^{-1} \times \sum_{t=1}^{d_k}\gamma_t\left(i,y^{(k)}\middle|\boldsymbol{\theta}_{\mathbf{old}},\zeta\right) \text{ x } \delta_{y_t^{(k)},q}\right)}{\sum_{k=1}^{K}\left(w_T^{(k)} \text{ x } \Pr\left(y^{(k)}\middle|\boldsymbol{\theta}_{\mathbf{old}},\zeta\right)^{-1} \times \sum_{t=1}^{d_k}\gamma_t\left(i,y^{(k)}\middle|\boldsymbol{\theta}_{\mathbf{old}},\zeta\right)\right)} \tag{4}$$

where $1 \le q \le m$.

In addition, the terms $\varepsilon_a^{(k)}(i,j,d|\boldsymbol{\theta},\zeta)$, $\kappa_a^{(k)}(r,j,d,y^{(k)}|\boldsymbol{\theta}_{old},\zeta)$ and $\gamma_t(i, y^{(k)}|\boldsymbol{\theta}_{old},\zeta)$ are introduced in order to simplify the MLE process and are defined as follows:

$$\varepsilon_a^{(k)}(i,j,d|\boldsymbol{\theta},\zeta) = \Pr\left(X_n = j, t_{a+d-1}^{(k)} < T_n \le t_{a+d}^{(k)}\middle| X_{n-1} = i, t_{a-1}^{(k)} < T_{n-1} \le t_a^{(k)}, \boldsymbol{\theta},\zeta\right),$$

$$\kappa_a^{(k)}\left(r,j,d,y^{(k)}\middle|\boldsymbol{\theta}_{old},\zeta\right) = \Pr\left(X_n = j, t_{a+d-1}^{(k)} < T_n \le t_{a+d}^{(k)}, X_{n-1} = i, t_{a-1}^{(k)} < T_{n-1} \le t_a^{(k)}, y^{(k)}\middle|\boldsymbol{\theta}_{old},\zeta\right),$$

$$\gamma_t\left(i,y^{(k)}\middle|\boldsymbol{\theta}_{old},\zeta\right) = Pr\left(Q_t = i, y^{(k)}\middle|\boldsymbol{\theta}_{old},\zeta\right),$$

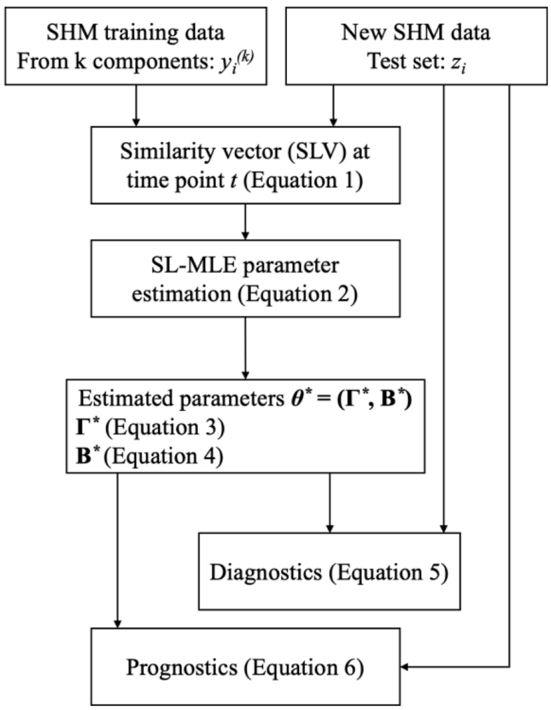

Fig. 1. Flowchart of the proposed Similarity Learning HSMM model.

with X_n being the state of the component after the nth transition, $T_n$the time of the nth transition, Q_t the current hidden state and $t_i^{(k)}$the ith observation time point of the kth observation sequence $y^{(k)}$ and $\delta_{y_t^{(k)},w}$ is equal to 1 when the tth observation value of $y^{(k)}$ is equal to q.

Starting from an initial assumption regarding setting initial values for $\mathbf{\Gamma}$, $\mathbf{B}$, defining the time step T and solving the aforementioned optimization problem i.e. $\sum_{k=1}^{K}\log(w_T^{(k)} \text{ x } \Pr(y^{(\mathbf{k})}|\boldsymbol{\theta},\zeta))$, the parameter estimation process is obtained.

It is worth mentioning that in the case of a noninformative and static SLV function, i.e. $w_T(k)= 1/K$ for every possible T and k, the SLHSMM is identical to the NHHSMM.

Table 1
Loading scenarios and resulted lifetimes of the tested panels.

Panel No	Minimum max Load (kN)	Maximum max Load (kN)	Life time (Fatigue cycles)
ca1	–	−65.0	280,098
ca2	–	−65.0	144,969
ca3	–	−65.0	133,281
ca4	−50.0	−65.0	259,500
va1	−40.0	−60.0	202,300
va2	−40.0	−55.0	243,000
va3	−40.0	−50.0	217,000
va4	−35.0	−60.0	345,000
va5	−40.0	−60.0	242,000
sp1	−50.4	−78.0	1580,000
sp2	−50.4	−78.0	529,000
sp3	−50.4	−82.0	1300,000
sp5	−45.9	−78.0	452,000
sp7	−45.9	−78.0	1160,460

2.2. Diagnostics

Finding a monotonic degradation measure, which at least reflects qualitatively the damage accumulation process has always been a challenging topic in SHM applications [34]. Finding such a monotonic measure will be critical in terms of defining the parameter T. To this end, a reasonable measure to monitor the overall health status of a composite structure is the diagnostic measure Most Likely State (MLS) [29], which can be determined via Eq. (5).

$$\text{MLS}(t|x_{1:t},\boldsymbol{\theta}^*,\zeta) = \underset{i}{\text{argmax}}\ \Pr(Q_t = i|x_{1:t},\boldsymbol{\theta}^*,\zeta) \quad (5)$$

This measure maximizes the probability $\Pr(Q_t = i|x_{1:t},\boldsymbol{\theta}^*,\zeta)$ of being at the hidden health state i at the time point t given the testing SHM data up to time t ($x_{1:t}$).

Utilizing the MLS diagnostic measure, the similarity learning time-step T can be defined as the transition timestep from the damage state N-2 to N-1, where N is the failure state. Following the aforementioned definition of T, a representative amount of data will be available in order to calculate the SLV vector. However, the number of degradation or health states N should be relatively small (N<10) so as to have enough time for decision-making and maintenance actions.

2.3. Prognostics

Prognostic measures can be defined based on the $\boldsymbol{\theta}$* model

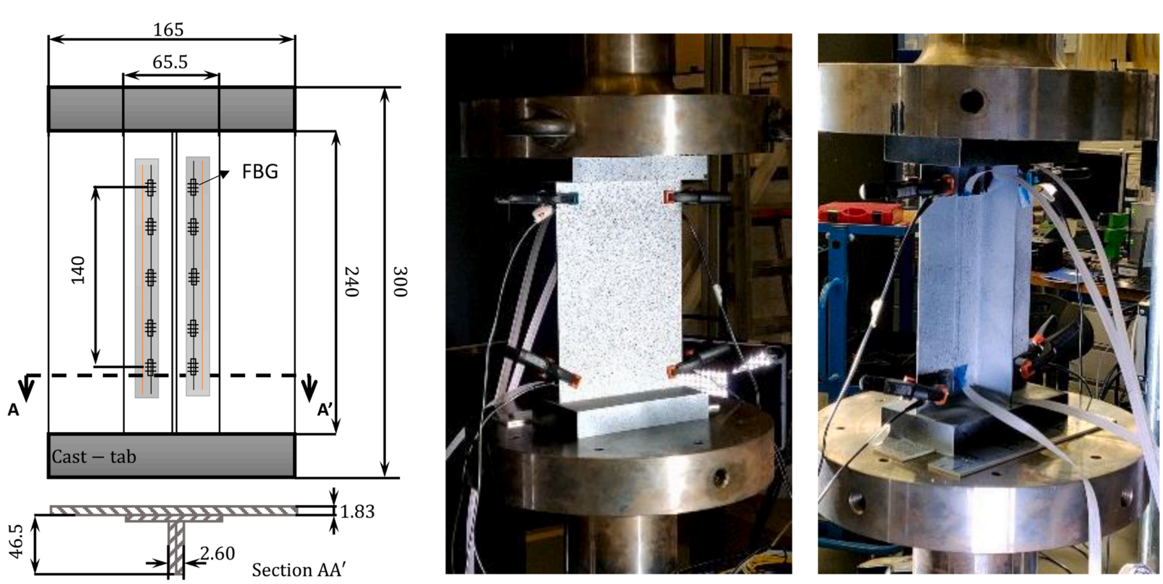

Fig. 2. A schematic representation of the panel and the experimental setup.

parameters and the testing SHM data ($\mathbf{x}$). Conditional to the testing SHM data and the complete similarity learning model parameters $\boldsymbol{\theta}^*$, prognostics aim to estimate the probability of being in degradation states 1, …,N-1 at a specific time points in the future, i.e., the conditional reliability function. Conditional reliability function, $\mathrm{R}(\mathrm{t}|\mathrm{x}_{1:\mathrm{t_p}}, L > \mathrm{t_p}, \boldsymbol{\theta}^*, \boldsymbol{\zeta}) = \Pr(L > t|x_{1:\mathrm{t_p}}, L > \mathrm{t_p}, \boldsymbol{\theta}^*, \zeta)$, represents the probability that the studied structure/asset continues to operate after a time t, less than the nominal life-time L ($L>t$), further than the current time $\mathrm{t_p}$, given that the structure has not failed yet ($L>$tp), the testing SHM data $\mathrm{x}_{1:\mathrm{tp}}$ and the complete model parameters $\boldsymbol{\theta}^*$, $\boldsymbol{\zeta}$.

The mean RUL as well as the uncertainty described by confidence intervals are proposed as the essential prognostic measures. These measures are calculated via the cumulative distribution function (CDF) of RUL [29]. The CDF of RUL is defined at any time point via the conditional reliability function according to the following equation:

$$\Pr\left(\mathrm{RUL}_{\mathrm{t_p}} \le t\middle|x_{1:\mathrm{t_p}}, \boldsymbol{\theta}^*, \boldsymbol{\zeta}\right) = 1 - R\left(t + \mathrm{t_p}\middle|\mathrm{x}_{1:\mathrm{t_p}}, \boldsymbol{\theta}^*, \boldsymbol{\zeta}\right) \tag{6}$$

Based on the above CDF of RUL and the application of Fubini's theorem, Eq. (7), which defines a random variable's mean value calculated directly from its CDF, the mean RUL value at time point $\mathrm{t_p}$ can be obtained from Eq. (8).

$$E[X] = \int_0^\infty (1 - F(x))\, dx - \int_{-\infty}^0 (F(x))\, dx \tag{7}$$

Where X is a random variable, F(X) is its CDF and E[X] its mean value.

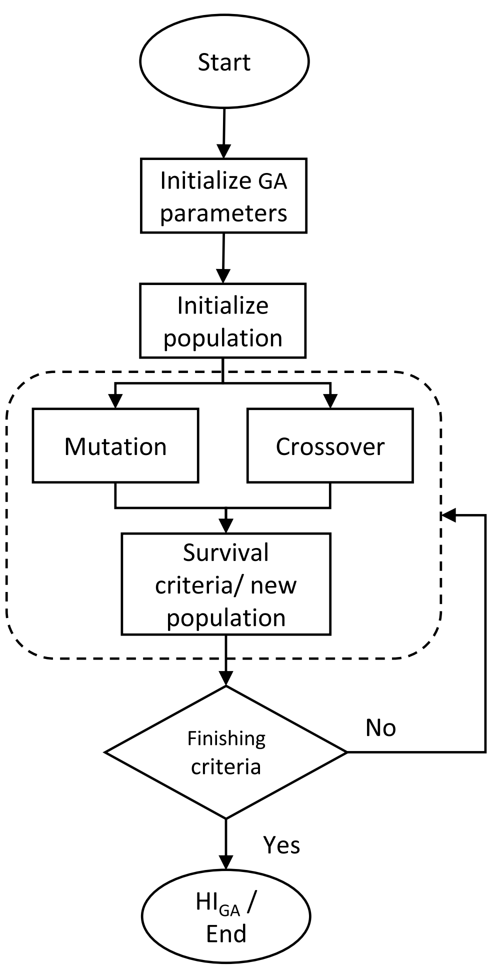

Fig. 3. Flowchart of the proposed Genetic algorithm HI fusion methodology.

$$E\left[\mathrm{RUL}_{\mathrm{t_p}}\right] = \int_0^\infty R\left(t + \tau\middle|y_{1:t_p}, L > t_p, \boldsymbol{\theta}^*, \boldsymbol{\zeta}\right) d\tau \tag{8}$$

3. Case-study

To demonstrate the adaptability and the efficiency of the proposed SLHSMM model, we employ it in SHM (strain) data obtained during a fatigue test campaign on carbon fiber reinforced polymeric panels, with a single stiffener. All panels host an initial damage at the area of the skin-stiffener interface in the form of a barely visible impact or an artificial disbond (Teflon insert during manufacturing). In the following we demonstrate how the SLHSMM is employed to estimate the RUL of composite panels utilizing SHM observations.

3.1. Experimental campaign

A series of experimental campaigns were performed at the Applied Mechanics Laboratory at the University of Patras and at the faculty of Aerospace Engineering at Delft Technical University. Each experimental campaign comprised a more complex loading scenario, starting from constant amplitude (CA), variable amplitude (VA), and finally random amplitude (spectrum (SP)) fatigue. All loads are in the compressive regime. The dimensions of the single-stringered panels are 300 × 165 mm^2 and the respective layups of the skin and stiffener are $[45/-45/0/45/90/-45/0]_S$ and $[45/-45/0/45/-45]_S$ made from Hexcel IM7/8552 UD prepreg. To ensure that the load is introduced uniformly, resin block tabs are cast into the free edges of the panels, creating a free length of 240 mm. A schematic representation of the panel and the experimental setup can be seen in Fig. 2.

Initially, the panels were tested at 65% of the compressive collapse load ($P = 100$ kN) with a frequency of 2 Hz and at a constant load ratio $R = 10$. However, as the experiments became more complex the load ratio was varying [35]. Table 1 summarizes the applied load range and the resulted fatigue lifetimes of the tested panels.

More information regarding the lifetimes and the applied loads can be found in [36]. We can clearly see that the failure time, especially for the spectrum panels, varies in a large range from 130 kcycles to almost 1600 kcycles.

The degradation of the panels is monitored, among other SHM systems, using strains recorded by 10 FBG sensors, 5 at each stiffener's foot, covering an area of approximately 140 mm at the center of the stiffener. The FBG sensors are encased in a SMARTape [37] which allows for a uniform strain transfer from the panel to the sensors. In the constant and variable amplitude fatigue campaigns, these strains are recorded every 500 cycles, during quasi-static loadings from the minimum to the maximum fatigue load [3,38]. For the spectrum test campaigns, the strains are recorded during fatigue every 7 min for a time window of 20 s [36].

3.2. Strain data processing

Strain data are collected from three different loading conditions. In order to collectively evaluate the degradation, the effect of the varying operational condition needs to be eliminated. To this end, methods to process the raw data have been proposed in [36,38]. These methodologies are mentioned here in brief for the sake of completeness. From the strains recorded during the quasi-static loadings (constant and variable amplitude campaigns) n measurements are uniformly sampled and averaged at each measurement instance. In the spectrum fatigue, during each 20 s measuring window, k random values are selected and averaged.

3.2.1. Health indicators development

Features capable of capturing the panels' degradation are essential

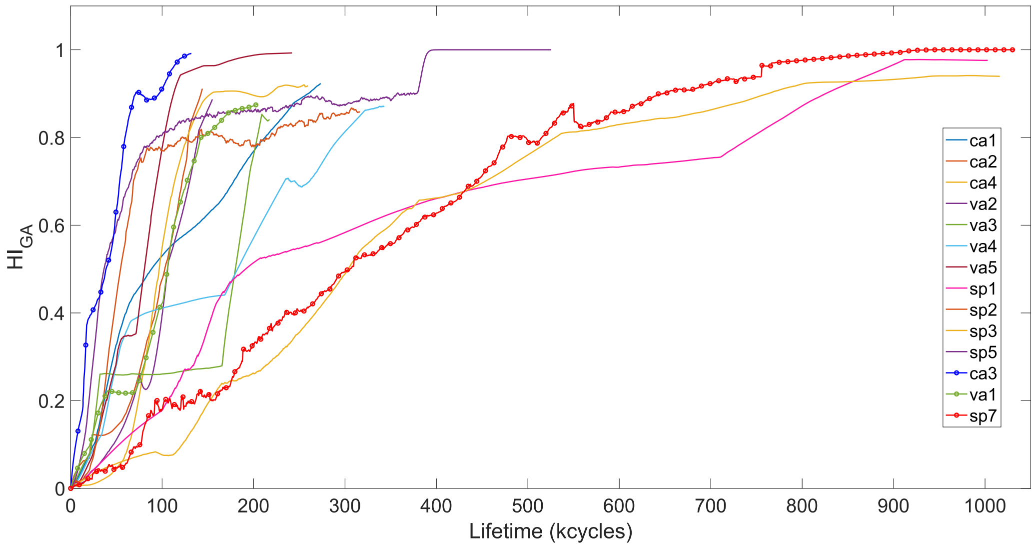

Fig. 4. Degradation feature (HI) histories for the training and testing panels vs fatigue life.

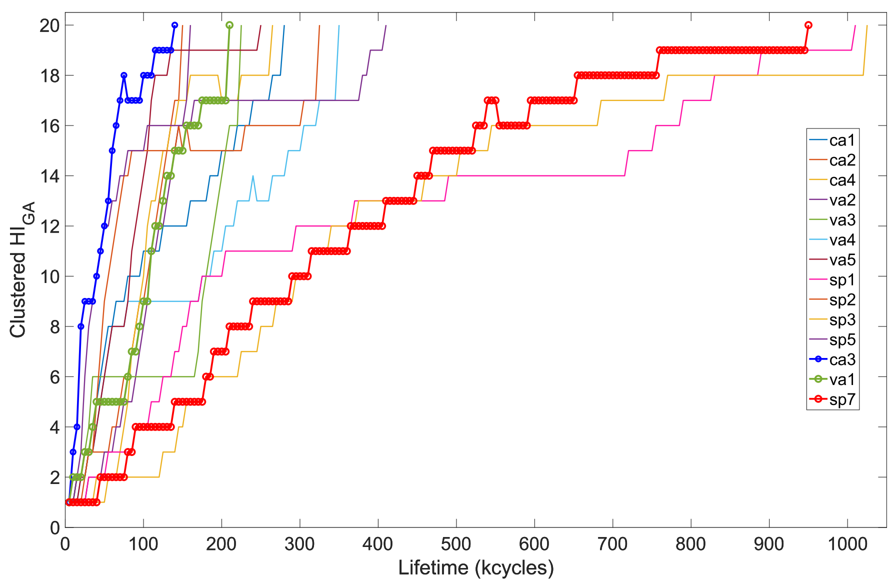

Fig. 5. Clustered $\mathrm{HI}_{\mathrm{GA}}$ degradation histories of training and testing panels.

for the task of RUL prognosis. As discussed in [25], the quality of the degradation features affects the performance and accuracy of the prognostic algorithms. We refer to these features as Health Indicators (HI). In previous works [36,38], strain-based HIs have been proposed for the purpose of monitoring the degradation of single stiffened panels. These HIs are briefly repeated here for the sake of completeness.

$$HI_1^i(t) = \frac{\left|\varepsilon_{ref}^i - \varepsilon^i(t)\right|}{\left|\varepsilon_{ref}^i\right|} \tag{9}$$

Evaluates the strain change at current time t relative to the reference stage (pristine or early SHM measurements). $\varepsilon^i(t)$ and ε_{ref}^i are the strain reading of sensor i at time t and reference state respectively

$$HI_2^i(t) = \frac{\varepsilon^i(t)}{\frac{\sum_1^n \varepsilon^i(t)}{n}} - \frac{\varepsilon^i(t=0)}{\frac{\sum_1^n \varepsilon^i(t=0)}{n}}, \ t > 0 \tag{10}$$

Indicates the proportion each FBG sensor contributes to the cumulative strain among the 10 FBG sensors of the same foot

$$HI_3(t) = \sqrt{\sum \left(M_i HI_1^i(t)\right)^2} \tag{11}$$

$$HI_4(t) = \sqrt{\sum \left(M_i HI_2^i(t)\right)^2} \tag{12}$$

HI_3 and HI_4 are a fusion of HI_1 and HI_2 for all FBG sensors, respectively, with weights being the monotonicity m_i of each HI_2^i curve.

$$\mathrm{vHI}_1(t) = \exp\left(-\frac{\left(d_L(t) - d_{Lmin}\right)^2}{\sigma_L}\right) \tag{13}$$

Where, $\sigma L = -\frac{\left(d_{Lmax} - d_{Lmin}\right)^2}{2}\left[\frac{1}{\log 10\varepsilon} + \frac{1}{\log 10(\varepsilon+\delta)}\right]$

The Euclidian distance is calculated as $d_L(t) = \| Z(t) - Z_0 \|$, where $Z(t)$ is the vector $[PC_1(t), PC_2(t)]$, where PC_1 and PC_2 are the first two principal components of a PCA. The HI is normalized via a radial basis function. ε and δ are scale parameters and are both set equal to 0.1. For the testing set, the normalization parameters are calculated from the training set.

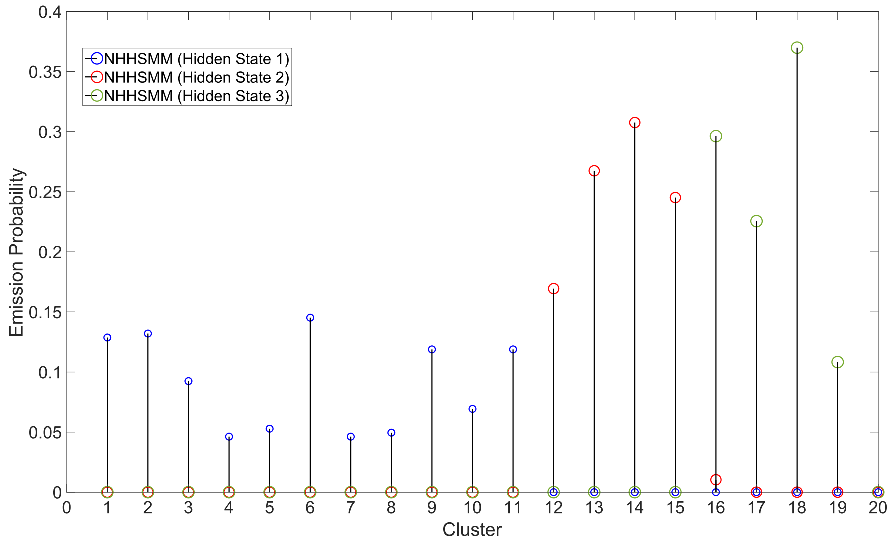

Fig. 6. NHHSMM **B*** emission probability parameters.

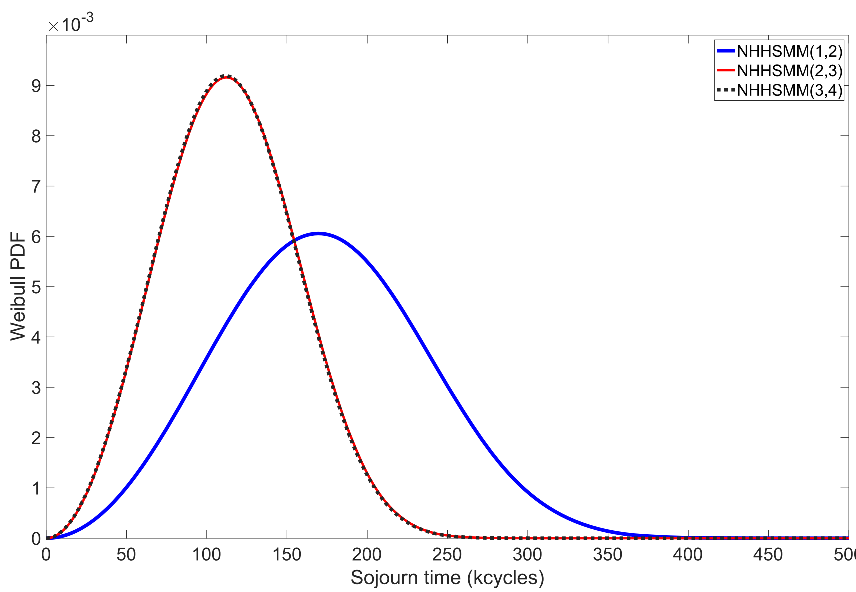

Fig. 7. Sojourn time Weibull distributions utilizing NHHSMM **Γ*** parameters.

$$vHI_2(t) = \sum_{1}^{N} \left(x_i(t) - x_{r_i}(t)\right)^2 \tag{14}$$

Which is a statistical quantity of PCA, also known as the squared sum of residual reconstructed error.

Since monotonicity and prognosability are crucial attributes of a candidate HI, a fusion methodology between simple HIs using genetic algorithms has been proposed. Genetic algorithms have been used by several researchers to discover prognostic features [39,40] since the process can be fully supervisable and easily understood [41]. The genetic algorithm receives as input the simple HIs and through genetic evolution it maximizes the sum average monotonicity and prognosability as defined in [42]. The allowed operations between HIs are addition, subtraction, multiplication, division, squared power, square root and logarithm. For the implementation, the GPLAB toolbox is used [43]. In Fig. 3a schematic representation of the HI development process is presented. The maximum number of iterations was set to 300 and the population of each generation to 150 since it was found to provide a good balance between performance and running time, while the maximum tree size (number of terms in the fusion equation) was set to 15 to avoid very complex equations. More detailed information on the fusion process can be found in [36,44].

The discovered fusion equation is:

$$HI = vHI_1\left(HI_4 - \frac{vHI_2 + 0.5HI_3}{vHI_2}\right) + 1 \tag{15}$$

The proposed by this process HI can be seen in Fig. 4 for all tested panels. Out of the 14 panels tested, 9 are kept for the training process whilst 5 are kept out of the genetic algorithm optimization. Two of these are used to validate the fusion process and three, i.e. ca3, va1, and sp7 constitute the test set upon which the RUL estimation methodologies are going to be tested. It is evident in Fig. 4 that even the test set histories display monotonic behaviors after the fusion process and the resulting HIs are highly prognosable with failure values very close to 1, which highlights the success of the optimization in improving prognosability.

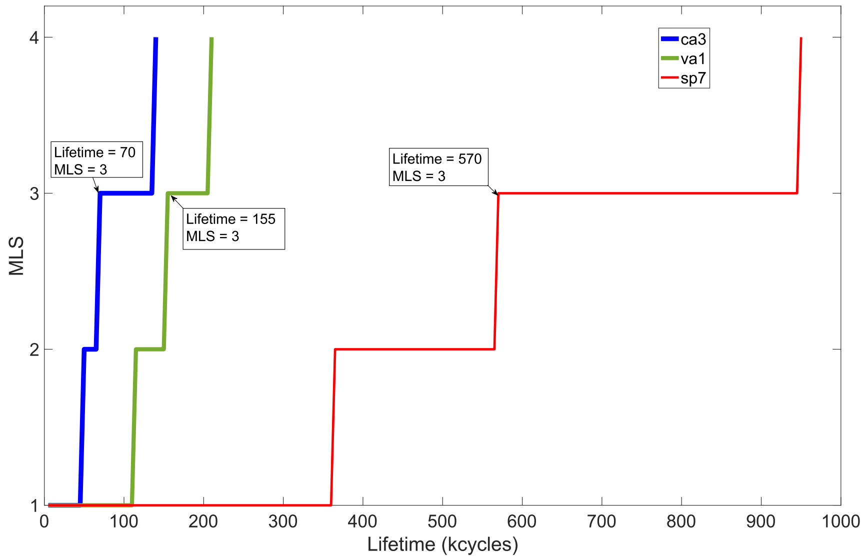

Fig. 8. MLS diagnostic measure of testing panels.

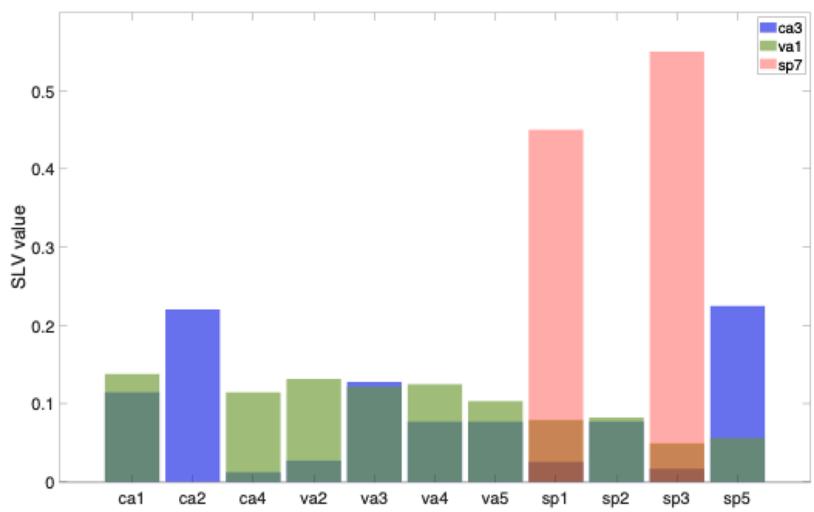

Fig. 9. Discrete similarity learning distributions of testing panels.

3.3. Similarity learning HSMM

Initially, the procedure of damage accumulation in composite panels under fatigue loading is modelled via the NHHSMM. The proposed parameter estimation process requires the initialization of parameters ζ = {N,Ω,λ,V}. The initialization parameters are defined as; the selected number of degradation states is four ($N = 4$) since based on Reifsnider and Talug [45] the damage accumulation process of composite structures can be approximated as a four-state process; the transition rate's statistical function (λ) from state i to state j, we assume a Weibull-type degradation and allow homogeneous transitions towards the neighborhood state (Ω: soft failures):

$$\lambda_{i,j}(t) = \frac{\beta_{i,j}}{a_{i,j}}\left(\frac{t}{a_{i,j}}\right)^{\beta_{i,j}-1} \quad if\ 1 \le i \le N-1,\ j = i+1 \tag{16}$$

where t is the sojourn time at state i, $a_{i,j}$ the scale and $\beta_{i,j}$ the shape Weibull parameters that characterize the soft transition from hidden state i to hidden state $j = i + 1$. Lastly, the training SHM data should be presented in a quantized form by V clusters, which can be estimated with the Modified Mann-Kendal (MMK) criterion [2]. After determining the number of clusters (V), the observation process (**B**) can be described using the emission matrix. The columns of this matrix correspond to the number of clusters V, while the rows correspond to the number of hidden states minus one. This is because the last hidden state is observed. The MMK converges quite well for a number of clusters equal to $V = 20$, as Figure A3 presents in the Appendix, and the final SHM data are presented in Fig. 5.

The goal of the NHHSMM is to estimate the observation process (**B**) and degradation process (**Γ**) parameters i.e. **θ***={**B***,**Γ***} parameters were determined via the SL-MLE procedure Eq. (2), defining the SLV vector as $w_T^{(k)} = 1/K$ where k ∈ [1,K]. In Fig. 6 and Fig. 7 the estimated NHHSMM **B*** and **Γ***parameters are presented accordingly.

The MLS diagnostic measure was calculated utilizing the estimated **θ*** parameters and the testing SHM data. Fig. 8 presents the estimations of the MLS measure as calculated from Eq. (5) at each time point during the operation time of the testing panels.

Based on the MLS estimations the similarity learning timestep T was defined for each testing panel, i.e. T_{ca3}=70 kcycles, T_{va1}=155 kcycles and T_{sp7}=570 kcycles, and the Euclidean SLV was obtained via Eq. (1). In Fig. 9, the SLV vectors for each testing panel are presented. As mentioned previously, the SLV represents the similarity of each testing panel with all the training panels. The calculation of this matrix enables

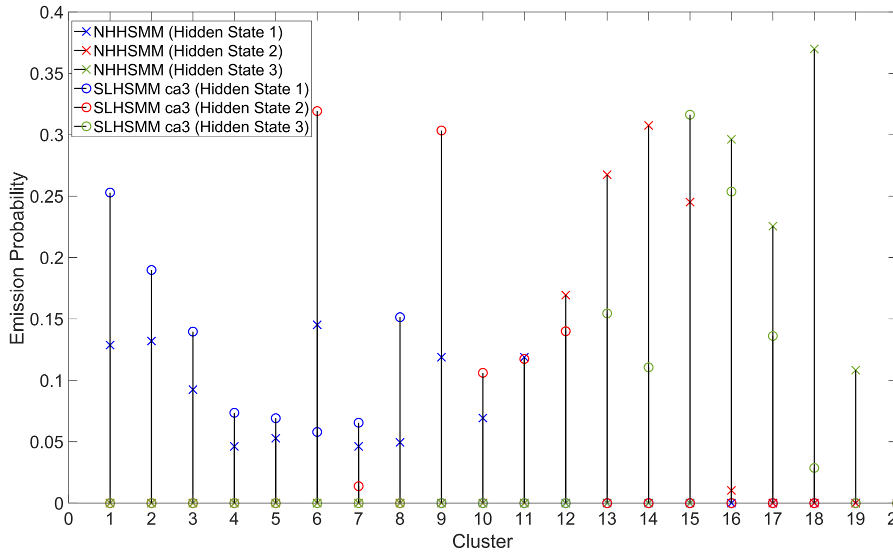

Fig. 10. Comparison between the training NHHSMM emission probability matrix (**B***) and the re-estimated emission probability matrix ($\mathbf{B}_{\mathbf{SLHSMM}}$*) of panel ca3.

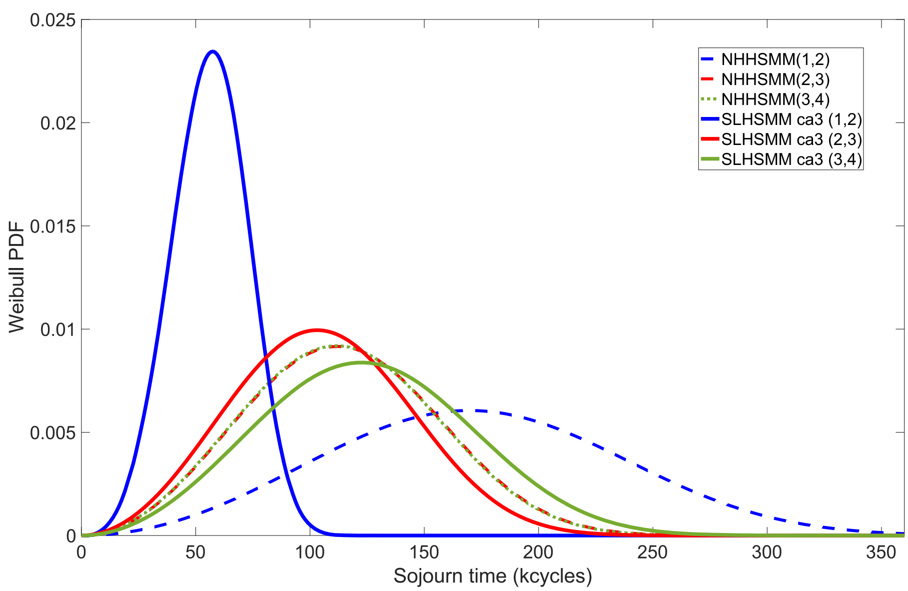

Fig. 11. Sojourn time Weibull distributions utilizing the NHHSMM $\mathbf{\Gamma}^*$ parameters and the $\mathbf{\Gamma}_{\mathbf{SL}}^{**}$ parameters of panel ca3.

the development of a training process that assigns greater importance to the training panels exhibiting higher similarity to the testing panel. To that end, utilizing such an approach the estimated parameters $\boldsymbol{\theta}^*$ can accurately capture the specific characteristics of the testing panel.

Based on Fig. 9 and Table 1 the testing panel ca3, i.e. the left outlier, has higher similarity with the training panels ca2 and sp5. Panel ca2 is the training set's left outlier case so it is desirable to observe such a correlation between the left outlier ca3 and the training set's left outlier. On the other hand, panel sp5 is a right-inlier case (closer to the right-outlier panel). This paradox occurs since the failure rate of panel sp5 is high at the beginning of its operation, Fig. 5. Regarding the panel va1 the similarity distribution is less informative, an observation that was expected since va1 is an inlier case. Finally, the testing panel sp7 is correlated only to two panels i.e. sp1 and sp2. These similarity-learning outcomes reflect that panel sp7 is closer to the training set's right outliers panels, sp1 and sp3.

Utilizing the testing SHM data and SLV vectors the SLHSMM can be defined and dynamically adapt the parameters $\boldsymbol{\theta}^*=\{\mathbf{B}^*, \mathbf{\Gamma}^*\}$ to $\boldsymbol{\theta}_{\mathbf{SL}}^*=\{\mathbf{B}_{\mathbf{SL}}^*, \mathbf{\Gamma}_{\mathbf{SL}}^*\}$, following the SL-MLE procedure Eq. (2). In Figs. 10 and 11, the outcomes of the SLHSMM regarding panel ca3 are presented and compared with the estimated NHHSMM parameters. The results of testing panels va1 and sp7 are presented in Figures A1 and A2 of the Appendix.

As Fig. 10 depicts the difference between the NHHSMM emission matrix (**B***) and the SLHSMM emission matrix ($\mathbf{B}_{\mathbf{SL}}$*) of panel ca3 is not negligible. For example, the probabilities $b_2(13)$, $b_2(14)$, $b_2(15)$, and $b_2(16)$ are equal to zero for the SLHSMM of panel ca3 but non-zero for the NHHSMM, the same observation can be extracted for some clusters of hidden state 1 and 3. To that end, it is worth mentioning that only the proposed SLHSMM, and not the ANHHSMM, is able to adapt the parameters of the emission matrix **B**. Finally, based on Fig. 11 the Similarity-Learning Weibull PDFs of panel ca3 for hidden states 1 and 2 are shifted to the left as was desired since panel ca3 has a shorter lifetime than the average training lifetime.

3.4. Remaining useful life estimations

Following the new similarity-learning framework, three four-state

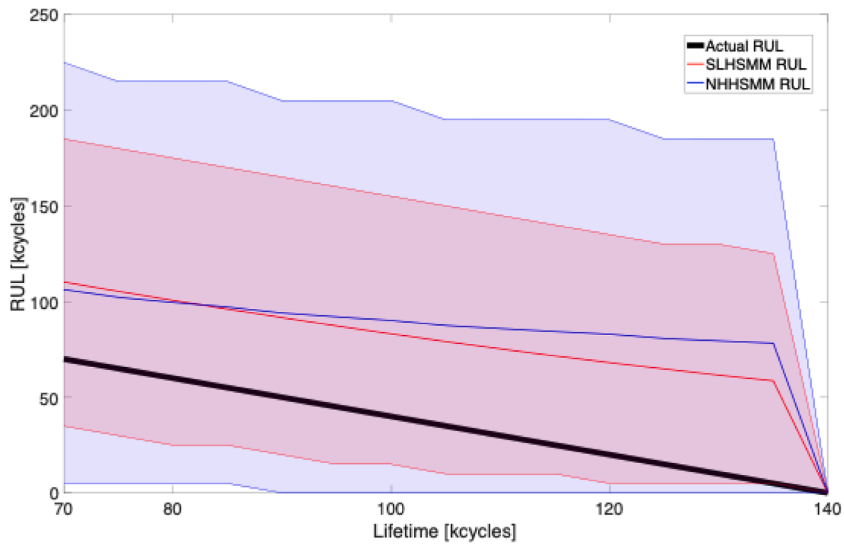

Fig. 12. RUL estimations of panel ca3 (left outlier).

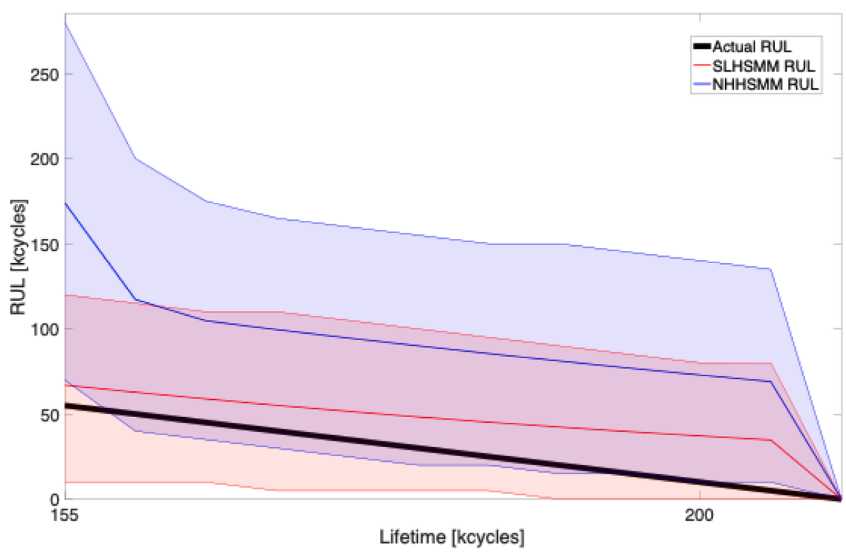

Fig. 13. RUL estimations of panel va1.

(N = 4) models, allowing soft state transitions, were developed and $\boldsymbol{\theta}^*$, $\boldsymbol{\theta}_{SL}^*=\{\boldsymbol{\theta}^*_{SL\text{-}ca3}, \boldsymbol{\theta}^*_{SL\text{-}va1}, \boldsymbol{\theta}^*_{SL\text{-}sp7}\}$ parameters were estimated according to the training and testing SHM data. Through Eq. (6), the conditional RUL CDF is calculated from the similarity learning timestep T, i.e., T_{ca3}=70 kcycles, T_{va1}=155 kcycles, and T_{sp7}=570 kcycles, till the end of life. The mean RUL and the 2.5 % and 97.5 % percentiles that define a 95 % CI are also highlighted. Figs. 12–14 present the RUL prognostic results of the SLHSMM and the NHHSMM for the test-set panels ca3, va1, and sp7 respectively. It is noted that the prognostics process starts after the last state transition (see Fig. 8) and not from the very beginning of the test as the new concept of SLHSMM dictates.

A simple visual check on Figs. 12–14 verifies the observation that the SLHSMM provides more accurate prognostics since the mean SLHSMM RUL estimations are able to approach the real RUL more as compared to the NHHSMM. Additionally, the confidence intervals of the SLHSMM contain the real RUL curve during the whole lifetime of panel sp7, and their width is generally shorter than the classic NHHSMM model.

3.5. Prognostic performance metrics

To further demonstrate the superiority of the newly developed SLHSMM model, a comparison was made with a Gaussian Process Regression (GPR) model, and the GPR RUL estimations are provided in Figures A4 to A6 in the Appendix. Detailed information about the GPR model can be found in [36], as it has been previously applied in this case study. Additionally, common prediction performance metrics, including MAE (mean absolute error), MAPE (mean absolute percent error), RMSE (root mean square error), and CRA (cumulative relative accuracy) for the mean RUL, are employed. Furthermore, MCIW (mean confidence interval width) and CICP (confidence interval coverage probability) for the confidence intervals [46,47] are utilized. The formulation of these metrics is presented in Eqs. (17)–(22):

$$MAE = \frac{1}{N}\sum_{i=1}^{N}\left|RUL_i - RUL_i^*\right| \tag{17}$$

$$MAPE = \frac{1}{N}\sum_{i-1}^{N}\frac{\left|RUL_i - RUL_i^*\right|}{RUL_i} \times \ 100 \tag{18}$$

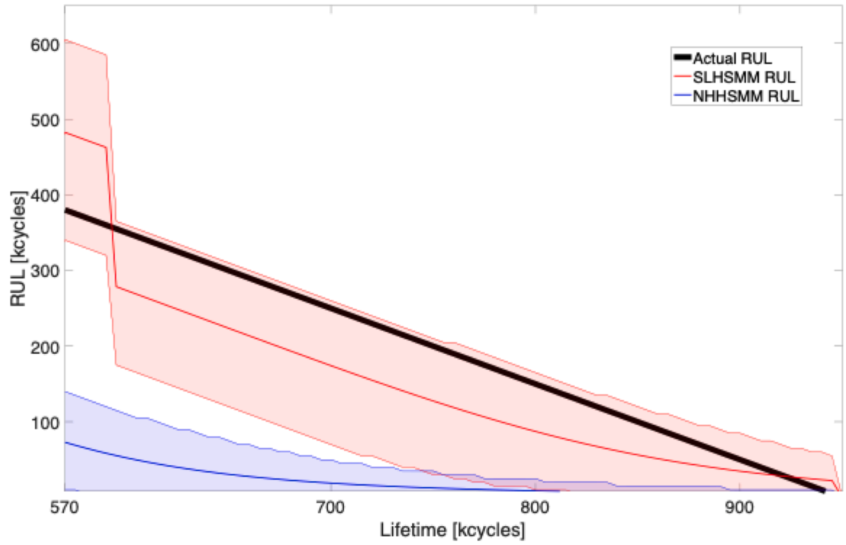

Fig. 14. RUL estimations of panel sp7.

Table 2
Prognostic performance metrics (with bold the most favorable value).

Coupon Name	Method	MAE (kcycles)	MAPE (%)	RMSE (kcycles)	CRA	MCIW (kcycles)	CICP (%)
ca3	GPR	175.89	240	209.31	−1.40	1675.39	100
	NHHSMM	52.56	289.85	53.86	−1.90	200.00	100
	SLHSMM	**42.91**	**214.58**	**43.06**	**−1.15**	**127.86**	100
va1	GPR	239.23	638	242.39	−5.38	1675.53	100
	NHHSMM	66.89	352.12	68.92	−2.52	142.27	82
	SLHSMM	**19.34**	**131.61**	**20.17**	**−0.32**	**94.55**	100
sp7	GPR	282.38	74	314.19	0.26	1675.52	100
	NHHSMM	172.81	88.70	196.91	**0.11**	**44.87**	3
	SLHSMM	**59.30**	**38.21**	**64.92**	0.62	157.30	100
AVERAGE METRICS							
	GPR	232.50	317.33	255.30	−2.17	1675.50	100
	NHHSMM	97.42	243.55	106.57	−1.44	129.05	61
	SLHSMM	**40.52**	**128.13**	**42.72**	**−0.28**	**126.57**	100

$$RMSE = \sqrt{\frac{1}{N}\sum_{i=1}^{N}\left(RUL_i - RUL_i^*\right)^2} \tag{19}$$

$$CRA = \frac{\sum_{i=1}^{N} RA_i}{N},\ where\ RA_i = 1 - \left|\frac{RUL_i - RUL_i^*}{RUL_i}\right| \tag{20}$$

$$MCIW = \frac{1}{N}\sum_{i=1}^{N}(U_i - L_i) \tag{21}$$

$$CICP = \frac{1}{N}\sum_{i=1}^{N}\xi_i \qquad Where\ \xi_i = \begin{cases} 1, & RUL_i \in [L_i, U_i] \\ 0, & otherwise \end{cases} \tag{22}$$

RUL_i and RUL_i^* are the true and predicted RUL at time i, and U_i and L_i the corresponding upper and lower bounds of the CIs. The comparative metrics can be seen in Table 2. It is evident that SLHSMM outperforms the NHHSMM and the GPR as it was also observed qualitatively from the RUL figures.

4. Conclusions

A new Similarity Learning Hidden Semi Markov model for prognostics is proposed in the present work aiming at more accurate predictions in cases of outlier behaviors unseen in the training data. The model was applied for the prognosis of the RUL of composite panels subjected to degradation during constant, variable, and random amplitude (spectrum) compression-compression fatigue experiments. FBG strain sensors, bonded at the stiffeners' feet, were used to monitor the condition of the panels during their lifetime. We utilized an advanced Health Indicator constructed out of strain data with the use of Genetic Algorithms, which proved capable of capturing the panels' degradation through lifetime. The results as quantified with common performance metrics clearly demonstrate that the SLHSMM provides superior prognostics as compared to the state-of-the-art NHHSMM and GPR all across the test set. We conclude that adapting the NHHSMM's parameters using the similarity learning vector as demonstrated in this work has the potential to predict the RUL of outlier and inlier cases more efficiently in terms of confidence intervals behavior and mean RUL accuracy. In addition, the proposed similarity-based model can dramatically reduce the training computational time due to its capability to showcase the important, in terms of similarity, degradation histories. For example, the testing panel sp7 at the time point T_{sp7}=570 kcycles defines that the training process can include data only from panels sp1 and sp3. To that end, only 23 % (2/11) of the available data will be used for the training process.

In conclusion, our proposed model demonstrates promising capabilities for predicting the RUL of composite panels. However, it is essential to acknowledge the main limitation of our model, which lies in the dependency between the Similarity Learning Vector (SLV) and the outliers present in the training set. This dependency, although present, has a relatively soft impact on RUL predictions, allowing our model to effectively handle outlier RUL cases. Another aspect to consider is the requirement of defining the similarity learning timestep T for calculating the SLV vector at specific moments. In our approach, we have defined the timestep T through diagnostics, marking the transition of the panel from one damage state to another. Consequently, the number of possible timesteps T is equal to the total number of states (N) minus one. Moving forward, we aim to automate the selection of the similarity learning timestep T by continuously calculating the similarity between the testing panel and the training panels. This will eliminate the need for manual definition and enhance the model's adaptability. Additionally, an area for improvement concerning the SVM vector lies in the calculation of similarity. Currently, we employ the Euclidean distance method for quantifying similarity, as presented in Eq. (1). However, the point-by-point formulation in Eq. (1) may not fully capture the complexities of the damage evolution processes. To overcome this limitation, our future research endeavors will focus on extending the point-by-point similarity formulation to a vector-to-vector formulation so as to facilitate a more comprehensive understanding and capture of the degradation process. Furthermore, it is important to note that the proposed new model effectively reduces the confidence intervals for RUL predictions. However, additional measures are required to further minimize them, thereby enhancing the model's applicability in real-life scenarios. It is worth mentioning that Markov models provide confidence intervals that focus primarily on the aleatoric uncertainty. As a result, emphasis should be placed on the quality of the data rather than solely on increasing the quantity.

Finally, it is worth noting that the proposed adaptive model exhibits high flexibility, enabling its potential application to various engineering prognostic problems.

Funding

The research work was supported by the Hellenic Foundation for Research and Innovation (H.F.R.I.) under the "First Call for H.F.R.I. Research Projects to support Faculty members and Researchers and the procurement of high-cost research equipment grant" (Project Number: 2573).

CRediT authorship contribution statement

Nick Eleftheroglou: Conceptualization, Methodology, Software, Formal analysis, Writing – original draft, Resources, Writing – review & editing. **Georgios Galanopoulos:** Investigation, Data curation, Writing – original draft, Resources, Writing – review & editing. **Theodoros Loutas:** Resources, Resources, Funding acquisition, Writing – original draft, Writing – review & editing.

Declaration of Competing Interest

The authors declare that they have no known competing financial interests or personal relationships that could have appeared to influence the work reported in this paper.

Data availability

Data will be made available on request.

Appendix

In this appendix the estimated **B*** (Fig. A1) and **Γ*** (Fig. A2) parameters of the NHHSMM and SLHSMM, the results of the MMK monotonicity criterion (Fig. A3), and the GPR prognostics for all the testing panels (Figs. A4–A6) are presented for clarity reasons.

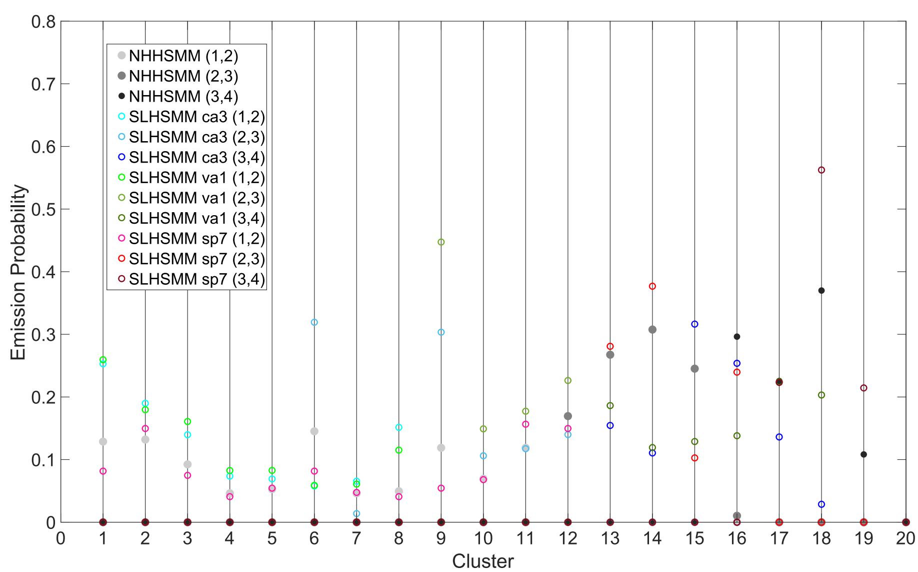

Fig. A1. NHHSMM (**B***) and SLHSMM (**B_{SL}***) emission probability matrices.

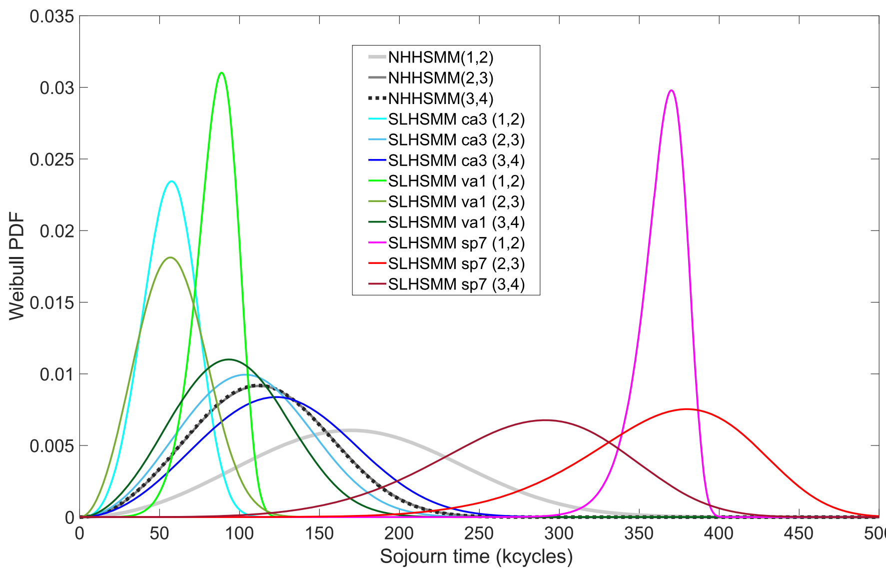

Fig. A2. Sojourn time Weibull distributions utilizing $\boldsymbol{\Gamma}^*$ and $\boldsymbol{\Gamma}_{SL}^{**}$ parameters.

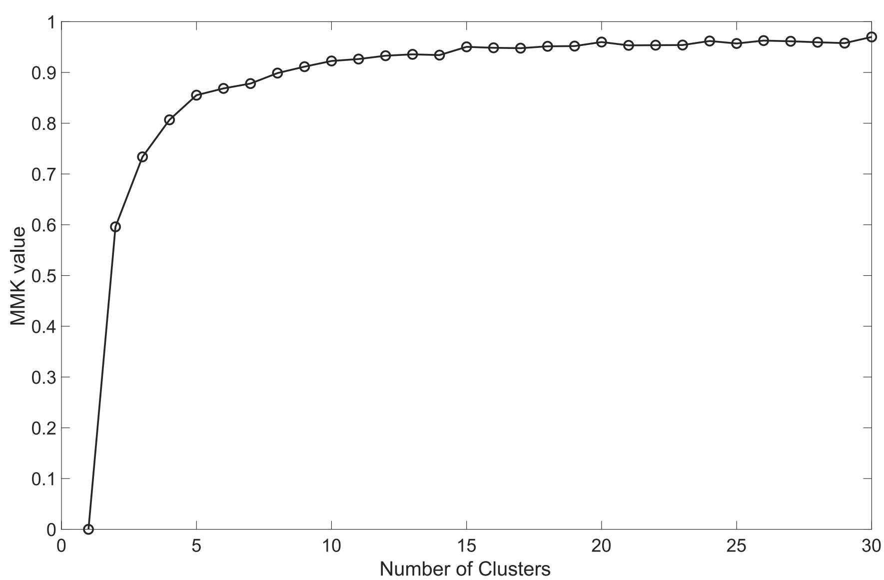

Fig. A3. MMK monotonicity convergence of the HI_{GA} data versus the number of clusters (V).

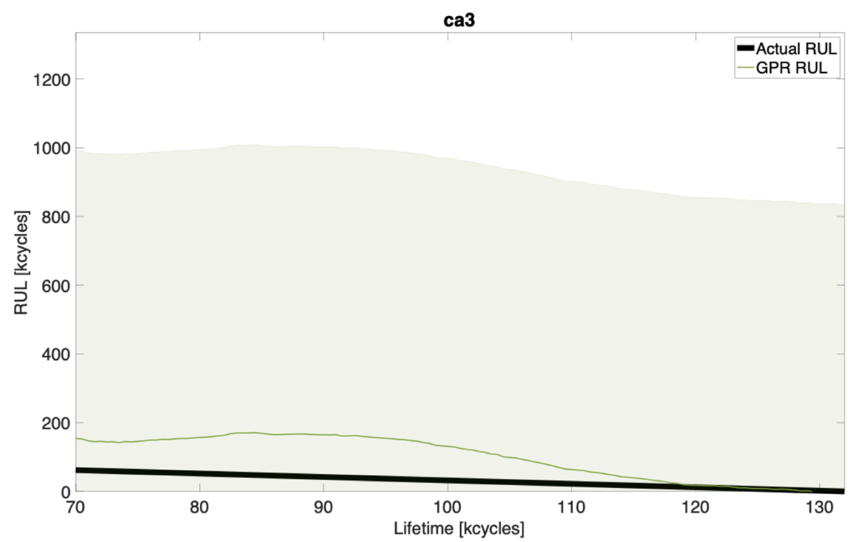

Fig. A4. GPR RUL estimations of panel ca3.

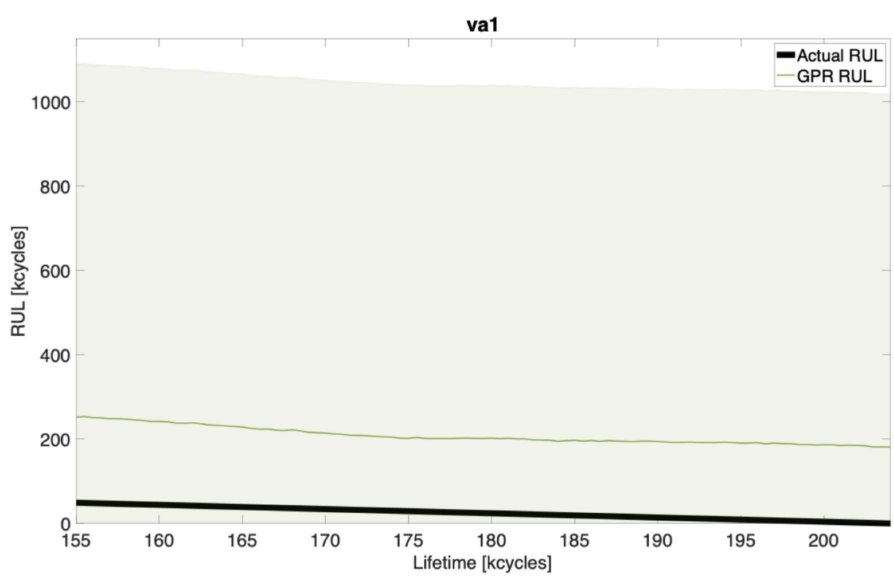

Fig. A5. GPR RUL estimations of panel va1.

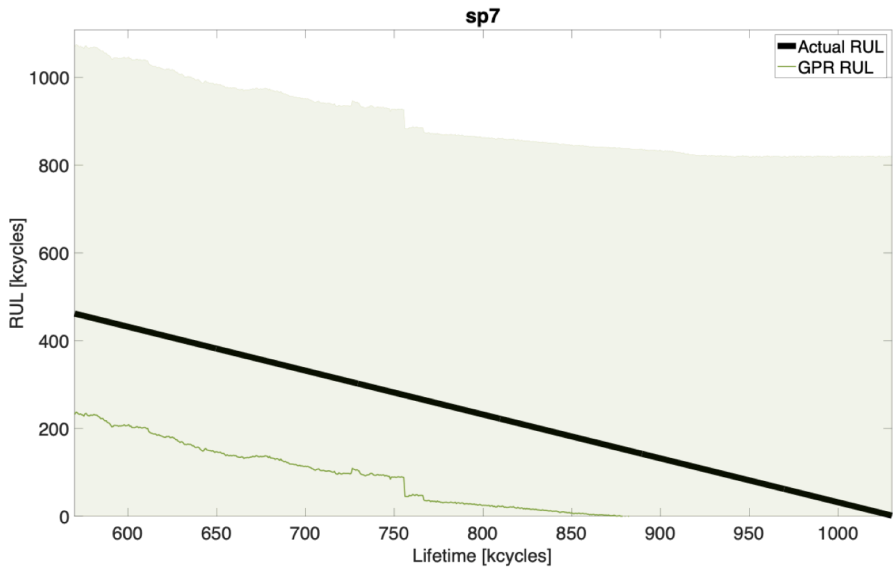

Fig. A6. GPR RUL estimations of panel sp3.

Table of Acronyms

AI	Artificial Intelligent
ANHHSMM	Adaptive Non-Homogeneous Hidden Semi Markov Model
CA	Constant Amplitude
CDF	Cumulative Density Function
CI	Confidence Interval
CM	Condition Monitoring
CRA	Cumulative Relative Error
EM	Expectation Maximization
GA	Genetic Algorithm
GPR	Gaussian Process Regression
HI	Health Indicator
MAE	Mean Absolute Error
MAPE	Mean Absolute Percentage Error
MCIW	Mean Confidence Interval Width
MLE	Maximum Likelihood Estimation
MLS	Most Likely State
MMK	Modified Mark Kendal
NHHSMM	Non-Homogeneous Hidden Semi Markov Model
PCA	Principal Component Analysis
PDF	Probability Density Function
pHI	physical Health Indicator
RBFNN	Radial Basis Function Neural Network
RMSE	Root Mean Squared Error
RUL	Remaining Useful Life
SHM	Structural Health Monitoring
SLHSMM	Similarity Learning Hidden Semi Markov Model
SL-MLE	Similarity Learning Maximum Likelihood Estimation
SLV	Similarity Learning Vector
SP	Spectrum
VA	Variable Amplitude
vHI	virtual Health Indicator

References

[1] Eleftheroglou N, Loutas T. Fatigue damage diagnostics and prognostics of composites utilizing structural health monitoring data and stochastic processes. Struct Heal Monit Int J 2016;15(4):473–88. https://doi.org/10.1177/1475921716646579.

[2] Eleftheroglou N, Zarouchas D, Loutas T, Alderliesten R, Benedictus R. Structural health monitoring data fusion for *in-situ* life prognosis of composite structures. Reliab Eng Syst Saf 2018;178:40–54. https://doi.org/10.1016/j.ress.2018.04.031.

[3] Broer A, Galanopoulos G, Benedictus R, Loutas T, Zarouchas D. Fusion-based damage diagnostics for stiffened composite panels. Struct. Heal. Monit. 2021 14759217211007128.

[4] Byington CS, Roemer MJ, Kacprzymki GJ, Galie T. Prognostic enhancements to diagnostic systems for improved condition-based maintenance. IEEE Aerosp Conf Proc 2002;6:2815–24.

[5] Loutas T, Eleftheroglou N, Zarouchas D. A data-driven probabilistic framework towards the *in-situ* prognostics of fatigue life of composites based on acoustic emission data. Compos Struct 2017;161:522–9. https://doi.org/10.1016/j.compstruct.2016.10.109.

[6] Eleftheroglou N, Zarouchas D, Benedictus R. An adaptive probabilistic data-driven methodology for prognosis of the fatigue life of composite structures. Compos Struct 2020;245:112386.

[7] Meng H, Geng M, Han T. Long short-term memory network with Bayesian optimization for health prognostics of lithium-ion batteries based on partial

incremental capacity analysis. Reliab Eng Syst Saf 2023;236:109288. https://doi.org/10.1016/j.ress.2023.109288.
[8] Zhuang L, Xu A, Wang XL. A prognostic driven predictive maintenance framework based on Bayesian deep learning. Reliab Eng Syst Saf 2023;234:109181. https://doi.org/10.1016/j.ress.2023.109181.
[9] Cao Y, Ding Y, Jia M, Tian R. A novel temporal convolutional network with residual self-attention mechanism for remaining useful life prediction of rolling bearings. Reliab Eng Syst Saf 2021;215:107813. https://doi.org/10.1016/j.ress.2021.107813.
[10] Chang Y, Chen J, Lv H, Liu S. Heterogeneous bi-directional recurrent neural network combining fusion health indicator for predictive analytics of rotating machinery. ISA Trans 2022;122:409–23. https://doi.org/10.1016/j.isatra.2021.04.024.
[11] Chang Y, Li F, Chen J, Liu Y, Li Z. Efficient temporal flow transformer accompanied with multi-head probsparse self-attention mechanism for remaining useful life prognostics. Reliab Eng Syst Saf 2022;226:108701. https://doi.org/10.1016/j.ress.2022.108701.
[12] Zhang SJ, Kang R, Lin YH. Remaining useful life prediction for degradation with recovery phenomenon based on uncertain process. Reliab Eng Syst Saf 2021;208:107440. https://doi.org/10.1016/j.ress.2021.107440.
[13] Zhang S, Zhai Q, Li Y. Degradation modeling and RUL prediction with Wiener process considering measurable and unobservable external impacts. Reliab Eng Syst Saf 2023;231:109021. https://doi.org/10.1016/j.ress.2022.109021.
[14] Pang Z, Li T, Pei H, Si X. A condition-based prognostic approach for age- and state-dependent partially observable nonlinear degrading system. Reliab Eng Syst Saf 2023;230:108854. https://doi.org/10.1016/j.ress.2022.108854.
[15] Yu W, Shao Y, Xu J, Mechefske C. An adaptive and generalized Wiener process model with a recursive filtering algorithm for remaining useful life estimation. Reliab Eng Syst Saf 2022;217:108099. https://doi.org/10.1016/j.ress.2021.108099.
[16] Liao G, Yin H, Chen M, Lin Z. Remaining useful life prediction for multi-phase deteriorating process based on Wiener process. Reliab Eng Syst Saf 2021;207:107361. https://doi.org/10.1016/j.ress.2020.107361.
[17] Orchard M, Tobar F, Vachtsevanos G. Outer feedback correction loops in particle filtering-based prognostic algorithms: statistical performance comparison. Stud Inform Control 2009;18(4):295–304.
[18] Sbarufatti C, Corbetta M, Giglio M, Cadini F. Adaptive prognosis of lithium-ion batteries based on the combination of particle filters and radial basis function neural networks. J Power Sources 2017;344:128–40.
[19] Khan F, Eker OF, Khan A, Orfali W. Adaptive degradation prognostic reasoning by particle filter with a neural network degradation model for turbofan jet engine. Data 2018;3(4):49.
[20] Daroogheh N, Baniamerian A, Meskin N, Khorasani K. A hybrid prognosis and health monitoring strategy by integrating particle filters and neural networks for gas turbine engines. In: Proceedings of the IEEE conference on prognostics and health management (PHM); 2015. p. 1–8.
[21] Si XS, Zhang ZX, Hu CH. Data-driven remaining useful life prognosis techniques. In: *Natl. Def. Ind.* Beijing, China: Press Springer-Verlag GmbH; 2017. https://doi.org/10.1007/978-3-662-54030-5.
[22] Gebraeel NZ, Lawley MA, Li R, Ryan JK. Residual-life distributions from component degradation signals: a Bayesian approach. IIE Trans 2005;37(6):543–57. https://doi.org/10.1080/07408170590929018. Institute Ind. Eng.
[23] Wang W, Carr M, Xu W, Kobbacy K. A model for residual life prediction based on Brownian motion with an adaptive drift. Microelectron Reliab 2011;51(2):285–93. https://doi.org/10.1016/j.microrel.2010.09.013.
[24] Cadini F, Sbarufatti C, Corbetta M, Cancelliere F, Giglio M. Particle filtering-based adaptive training of neural networks for real-time structural damage diagnosis and prognosis. Struct Control Heal Monit 2019;26(12):e2451.
[25] Loutas T, Eleftheroglou N, Georgoulas G, Loukopoulos P, Mba D, Bennett I. Valve failure prognostics in reciprocating compressors utilizing temperature measurements, PCA-based data fusion, and probabilistic algorithms. IEEE Trans Ind Electron 2019;67(6):5022–9.
[26] Baum LE, Petrie T. Statistical inference for probabilistic functions of finite Markov chains. Ann Math Stat 1966;73:1554–63.
[27] Rabiner LR. A tutorial on hidden Markov models and selected applications in speech recognition. Proc IEEE 1989;77(2):257–86.
[28] Peng Y, Dong M. A prognosis method using age-dependent hidden semi-Markov model for equipment health prediction. Mech Syst Signal Process 2011;25(1):237–52.
[29] Moghaddass R, Zuo MJ. An integrated framework for online diagnostic and prognostic health monitoring using a multistate deterioration process. Reliab Eng Syst Saf 2014;124:92–104.
[30] Peng Y, Dong M. A prognosis method using age-dependent hidden semi-Markov model for equipment health prediction. Mech Syst Signal Process 2011;25(1):237–52.
[31] Orchard ME, Vachtsevanos GJ. A particle-filtering approach for on-line fault diagnosis and failure prognosis. Trans Inst Meas Control 2009;31(3–4):221–46.
[32] Bogdanoff JL, Kozin F, Saunders H. Probabilistic models of cumulative damage. J Vib Acoust Stress Reliab Des 1988;110(4):575–6. https://doi.org/10.1115/1.3269574. Oct.
[33] XiaoFei L, Min L. Hazard rate function in dynamic environment. Reliab Eng Syst Saf 2014;130:50–60.
[34] Shen Z, He Z, Chen X, Sun C, Liu Z. A monotonic degradation assessment index of rolling bearings using fuzzy support vector data description and running time. Sensors 2012;12(8):10109–35.
[35] De Jong JB, Schütz D, Lowak H, Schijve J. A standardized load sequence for flight simulation tests on transport aircraft wing structures,. NLR-TR 73029U, LBF Bericht FB-106 1973. http://resolver.tudelft.nl/uuid:de6e293c-034f-426d-b842-3229268fd7ac.
[36] Galanopoulos G, Eleftheroglou N, Milanoski D, Broer A, Zarouchas D, Loutas T. A novel strain-based health indicator for the remaining useful life estimation of degrading composite structures. Compos Struct 2023;306:116579. https://doi.org/10.1016/J.COMPSTRUCT.2022.116579. Feb.
[37] Glisic B, Inaudi D. Development of method for in-service crack detection based on distributed fiber optic sensors. Struct Heal Monit An Int J 2011;11(2):161–71. https://doi.org/10.1177/1475921711414233.
[38] Galanopoulos G, Milanoski D, Broer A, Zarouchas D, Loutas T. Health monitoring of aerospace structures utilizing novel health indicators extracted from complex strain and acoustic emission data. Sensors 2021;21(17):5701.
[39] Firpi H, Vachtsevanos G. Genetically programmed-based artificial features extraction applied to fault detection. Eng Appl Artif Intell 2008;21(4):558–68. https://doi.org/10.1016/j.engappai.2007.06.004. Jun.
[40] Liao L. Discovering prognostic features using genetic programming in remaining useful life prediction. IEEE Trans Ind Electron 2014;61(5):2464–72. https://doi.org/10.1109/TIE.2013.2270212.
[41] Nguyen KTP, Medjaher K. An automated health indicator construction methodology for prognostics based on multi-criteria optimization. ISA Trans 2021;113:81–96. https://doi.org/10.1016/j.isatra.2020.03.017. Jul.
[42] Coble J, Hines JW. Identifying optimal prognostic parameters from data: a genetic algorithms approach. In: Proceedings of the annual conference of the PHM society. 1; 2009.
[43] Silva S, Almeida J. GPLAB-a genetic programming toolbox for MATLAB. In: Proceedings of the Nordic MATLAB conference; 2003. p. 273–8.
[44] Galanopoulos G, Eleftheroglou N, Milanoski D, Broer A, Zarouchas D, Loutas T. An SHM data-driven methodology for the remaining useful life prognosis of aeronautical subcomponents. Lect Notes Civ Eng 2023;253:244–53. https://doi.org/10.1007/978-3-031-07254-3_24. LNCE.
[45] Reifsnider KL, Talug A. Analysis of fatigue damage in composite laminates. Int J Fatigue 1980;2(1):3–11.
[46] Saxena A, Celaya J, Saha B, Saha S, Goebel K. Metrics for offline evaluation of prognostic performance. Int J Progn Heal Manag 2010;1(1):4–23.
[47] Oikonomou A, Eleftheroglou N, Freeman F, Loutas T, Zarouchas D. Remaining useful life prognosis of aircraft brakes. Int J Progn Heal Manag 2022;13(1). https://doi.org/10.36001/IJPHM.2022.V13I1.3072. Jan.